Electron density measurement of a colliding plasma using soft-x-ray laser interferometry

A. S. Wan, T. W. Barbee, Jr., R. Cauble, P. Celliers, L. B. Da Silva, J. C. Moreno, P. W. Rambo, G. F. Stone, J. E. Trebes, and F. Weber

Lawrence Livermore National Laboratory, P.O. Box 808, Livermore, California 94550

(Received 9 January 1997)

We have used a soft-x-ray laser interferometer to study the collision and subsequent interaction of counterstreaming high-density plasmas. The measured density profiles show the evolution of the colliding plasmas from interpenetration, when the low-density edge of the plasmas first collide, to stagnation at the symmetry plane with density building at the symmetry plane. We compare the measured profiles with density profiles calculated by the radiation hydrodynamic code LASNEX, which predicts plasma stagnation as soon as the plasmas collide, and a particle-in-cell code, which allows for interpenetration, softening the stagnation. [S1063-651X(97)09505-6]

PACS number(s): 52.70.La, 42.55.Vc, 52.20.Hv, 52.25.Nr

The understanding of the collision and subsequent interaction of counterstreaming high-density plasmas is important for the design of inertial confinement fusion (ICF) hohlraums [1,2]. In a typical cylindrical indirectly driven ICF vacuum hohlraum, the interaction of the optical laser drive with high-Z (typically Au) inner hohlraum surface generates high-density counterstreaming plasmas that flow unimpeded and collide on the axis of the hohlraum. Single-fluid Lagrangian radiation hydrodynamics codes that we typically use to design ICF and other laser-plasma experiments, such as LASNEX [3], do not allow for plasma interpenetration. Without interpenetration, as the plasmas collide and stagnate, their kinetic energy converts to internal energy, resulting in an unphysically large ion temperature (T_i) and strong shocks that propagate away from the axis of symmetry. Furthermore, as the plasma stagnates, single-fluid codes predict the creation of jets of high-velocity and high-density plasmas, which can stream toward the ICF capsule located at the center of the hohlraum and destroy the symmetry of the capsule implosion before ignition. Current hohlraum designs for Nova [1,2,4] and the point design for the National Ignition Facility [1,2,5] employ a low-density fill gas to impede the plasma blowoff from stagnating on the hohlraum axis before the capsule ignition.

Past experimental studies of colliding plasmas have primarily focused on laser-produced, low-Z (Al, Si) front-illuminated thick targets [6–12] and back-illuminated exploding thin foils [8,13]. Most of the experiments utilized x-ray spectroscopy and imaging techniques to characterize the plasma parameters. Electron temperatures (T_e) were determined through line ratios and ionization balance, and T_i through line shapes. Electron densities (n_e) were estimated by line ratios [10] and holographic interferometry at 2630 Å [6]. Elton *et al.* [12] presented a description of the typical usage of a set of diagnostics described above to characterize front-illuminated Al slabs.

We used soft-x-ray laser interferometry [14,15] to study the evolution of colliding plasmas in an ICF-relevant regime by determining two-dimensional (2D) n_e profiles at different times. The interferometry system consists of a collimated x-ray laser source, an imaging mirror, and a skewed Mach-Zehnder interferometer consisting of two flat multilayer mirrors and two multilayer beam splitters. In contrast to conventional optical interferometers [6], we use a collisionally pumped Ne-like Y x-ray laser operating at 155 Å as the probe source. The order of magnitude reduction of the wavelength of the probe laser allows us to obtain a 2 order of magnitude improvement in spatial resolution due to reduced refraction and a 2 to 3 order of magnitude enhancement in signal strength due to reduced absorption. The short pulse duration ($\sim$200 ps) and high brightness of the x-ray laser allowed us to obtain data with reduced motion blurring. The beam splitters used in the interferometer are the most critical element of the system. They were not perfectly flat, creating some minor variations in the unperturbed fringe pattern and one of our dominant experimental uncertainties. Based on previous null shots with similar quality beam splitters, we estimate the uncertainty to be of order 0.1 fringe.

The setup of our colliding plasma experiment is shown in Fig. 1. Two Au slabs were aligned at 45° with respect to the symmetry plane. The distance at the minimum gap (in the y direction shown in Fig. 1) between the tips of the two slabs is defined as D_{gap}. We used a 500-μm full-width line-focused laser beam ($\lambda_{\mathrm{laser}}=0.53$ μm), originating from the $+x$ direction shown in Fig. 1, that irradiated the slabs and generated the counterstreaming plasmas. The laser had an intensity on target of 3×10^{14} W/cm^2 with a 1-ns-long temporally square pulse shape. At late time the two plasma streams collided at the symmetry plane. By varying the ge-

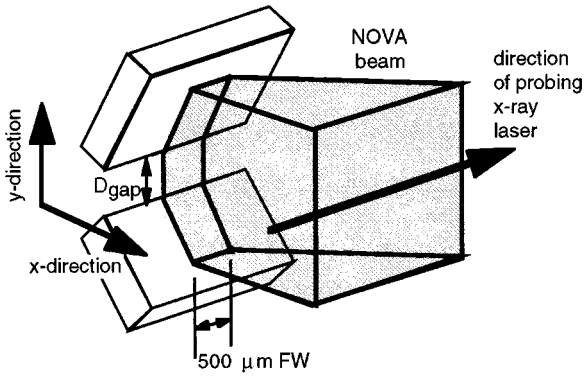

FIG. 1. 3D view of the experimental configuration for the colliding plasma experiment, with x and y definitions.

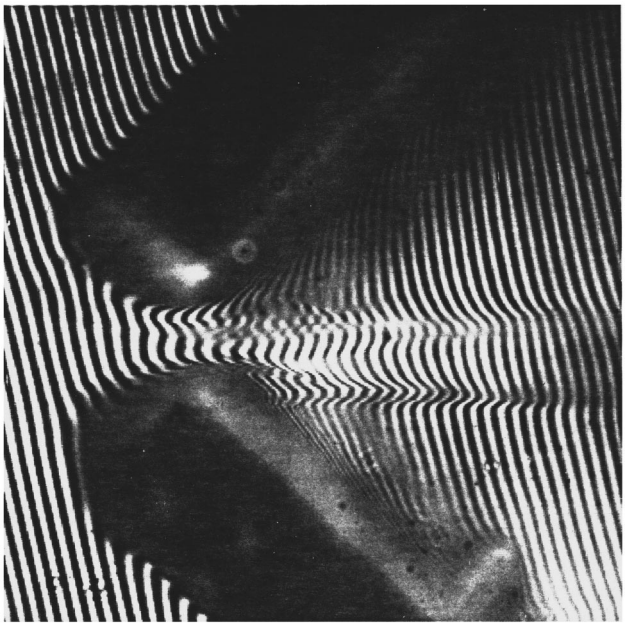

FIG. 2. (Color) Interferogram of two colliding gold plasmas from a 250-μm-gap target probed at 1.0 ns.

ometry, the slab materials, and the intensity of the incident optical laser, we were able to change the collisionality of the plasma and observe the evolution of the colliding plasmas. For a 50-times-ionized Au plasma with $T_e \sim 2$ keV and $n_i \sim 10^{19}$ cm^{-3}, the ion-ion mean free path of $\sim 100\ \mu$m is smaller than the system dimension of our target. For lower densities and higher temperatures, the plasma is less collisional and significant plasma interpenetration is expected. By using a He-Ne laser as an alignment light source in place of the x-ray laser, we obtained an image of the target prior to the shot so we have good knowledge of the initial slab positions.

We have conducted three experiments: two experiments with $D_{\text{gap}} = 500\ \mu$m, one probed at 0.6 ns into the pulse, and the other probed at 1 ns, and one experiment with a narrower gap of $D_{\text{gap}} = 250\ \mu$m probed at 1 ns. In Fig. 2 we show the interferogram from the latter case. The image shows excellent fringe visibility with distinct regions of fringe shifts corresponding to local density maxima. At the extreme edges of the interferogram, where there is no plasma, we observe unperturbed fringes. We use these fringes to construct an unperturbed 2D fringe map that is used to reference the overall fringe shift pattern. At any point, the number of fringe shifts is equal to $(n_e L)/(2 n_{\text{cr}} \lambda_{\text{XRL}})$, where λ_{XRL} is the x-ray laser wavelength, L is the path length across the target plasma, and n_{cr} is the corresponding critical density at 155 Å (4×10^{24} cm^{-3}). The uncertainty of the path length in the direction of the collimated x-ray laser beam can be significant for a narrow line-focused target since plasma expands in 3D [15]. In this paper we assume a uniform plasma with $L = 500\ \mu$m, which is the transverse width of the optical laser line focus.

Figure 3 shows the 2D n_e profile corresponding to the interferogram of Fig. 2. At the central region between the two slabs, there is a significant density buildup due to plasma collision and subsequent stagnation. For this narrow gap target, in the stagnation region we observe n_e peaks $\sim 40\ \mu$m off the symmetry plane with maximum densities of $\sim (6-8) \times 10^{20}$ cm^{-3}. The symmetry plane of the colliding plasmas is not at the center of the two slabs due to slight nonuniform irradiation parallel to the line focus (in the y direction). For our data analyses we placed the position of the symmetry plane at the midpoint between the peaks of the n_e maximum in Fig. 2.

The solid line of Fig. 4(a) is a 1D cut along the y direction at $x = 250\ \mu$m in Fig. 3. The error bar reflects the experimental uncertainty, primarily due to quality of the beam splitter. Uncertainty due to data fitting is minimal because of excellent fringe visibility. Results of the other two experiments are also shown. The $D_{\text{gap}} = 500\ \mu$m (1 ns) result reveals an

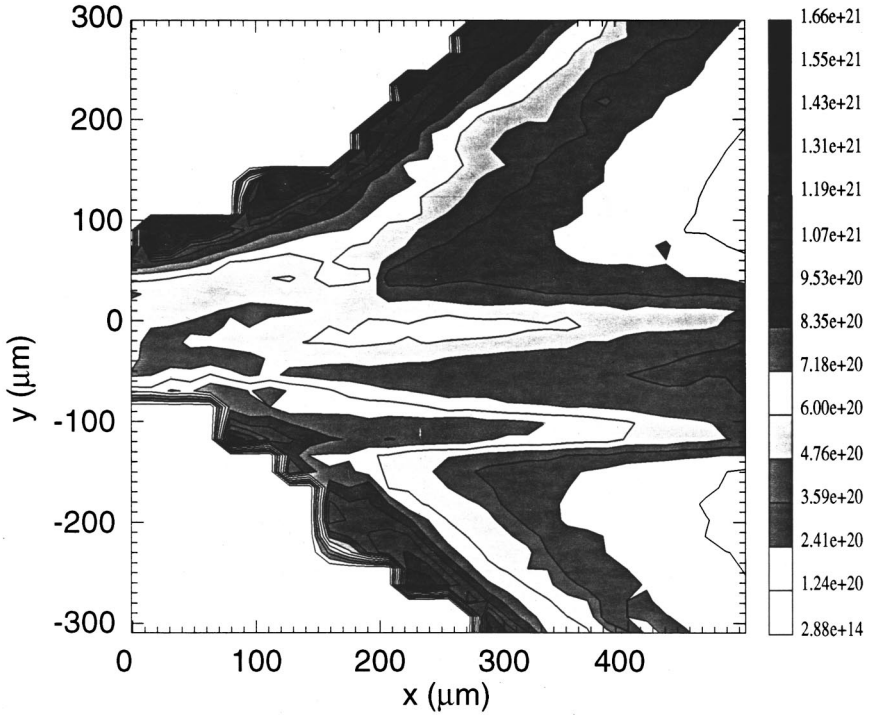

FIG. 3. (Color) Measured 2D n_e profile for a 250-μm-gap target with the peaked n_e regions away from the symmetry plane. Data are from interferogram shown in Fig. 2.

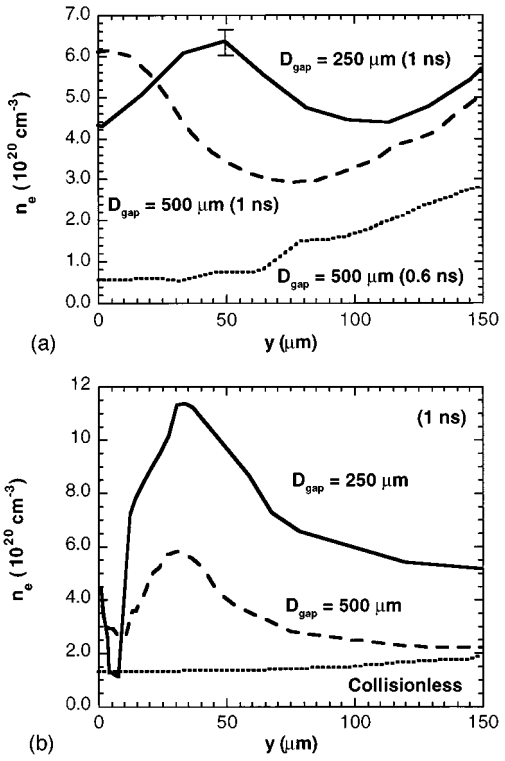

FIG. 4. 1D lineouts of (a) measured and (b) LASNEX-calculated n_e profiles at a position defined by $x=250$ μm, taken perpendicular to the symmetry plane. The solid line represent the profile with $D_{\text{gap}}=250$ μm, probed at 1 ns; the dashed line is the profile from the $D_{\text{gap}}=500$ μm target also probed at 1 ns. The dotted line is from the $D_{\text{gap}}=500$ μm target probed at 0.6 ns. The dotted line for Fig. 4(b) represents calculated profile with plasmas in a collisionless regime.

n_e profile peaking at the symmetry plane and with a maximum n_e of $\sim 6\times 10^{20}$ cm^{-3}; this is shown as the dashed curve in Fig. 4(a). The profile from the 500-μm-gap (0.6 ns) target, shown as the dotted curve, showed no density buildup, even though the low-density plasma fronts have begun to overlap. This is evidence for early time plasma interpenetration.

At late times (1 ns probes), there is significant density buildup at the symmetry plane as the counterstreaming plasmas collide and stagnate. The early time (0.6 ns) sequence shows no buildup even though the low-density plasma fronts have already begun to interact. This experimental observation of the evolution from early time interpenetration to later time stagnation at the symmetry plane points to the problem of using Lagrangian hydrodynamics codes to model such a system.

With two different gap separations, we observe very different density profiles at the stagnation region in late time. With the larger gap (500 μm), n_e peaks on axis. With the 250-μm gap, we observe two off-axis n_e peaks, suggestive of outward propagating shocks. In a parallel target geometry, the increased target separation delays the stagnation time due to the increased transit time [16,17]. We can qualitatively correlate the change in gap width with viewing different stages of the plasma collision—the narrower gap corresponds a later time in the collision. Putting these three shots into a temporal sequence characterizing the evolution of the collision, we first observe plasma interpenetration at early time, followed by large density buildup at the symmetry plane, indicating a soft plasma stagnation with density peaking on axis, and finally at late time, some evidence of outward propagating shocks.

A strong motivation to perform the colliding plasma experiment is to examine the validity of simulation and design codes, such as LASNEX, in a regime that might deviate from the fluid behavior. Jones *et al.* [18] give an excellent overview of various computational techniques used to model interpenetration, stagnation, and thermalization of colliding plasmas. We have performed 2D LASNEX calculations to simulate the colliding plasma configuration shown in Fig. 1. For these calculations a mirror reflectivity boundary condition was set at the symmetry plane. As the blowoff plasma reaches the symmetry plane, the velocity of the zone boundary for a Lagrangian code is set equal to zero, and the stagnation of the counterstreaming single-fluid plasmas results in the conversion of kinetic to internal energy. In this case LASNEX calculates an unphysically large T_i (exceeding 10^3 keV) similar to the 1D Lagrangian solution calculated by Berger *et al.* [8]. This high T_i results in shocks that propagate away from the symmetry plane, resulting in higher-density regions peaking off the symmetry plane.

These simulations used a multigroup radiation diffusion method to account for radiative effects. In the blowoff plasma, T_e is as high as 3 keV. However, due to the 2D nature of LASNEX, the direction along the 500-μm linewidth (see Fig. 1) is optically thick. This assumption causes a significant overestimate of the heating and results in higher temperatures. Using an approximation in which the radiation is optically thin in all directions, LASNEX predicts T_e ~ 1.0 keV. Measured T_e from past experiments [19] of simple Au disks indicate T_e of order 1.7–2.0 keV at this irradiation condition. The change in the plasma parameters significantly impacts the ionization balance, hydrodynamics, and collisionality of the plasma.

Figure 4(b) is a plot of 1D lineouts from 2D LASNEX calculations that can be compared with the data shown in Fig. 4(a). The dotted line in Fig. 4(b) was formed by superposing two independent plasma expansion simulations and is meant to represent complete interpenetration. Without stagnation the n_e profile shows a minimum at the symmetry plane, similar to our early time measurement. In the single-fluid limit, the LASNEX calculations predict n_e profiles that peak off the symmetry plane, characteristic of the stagnation profile predicted by single fluid Lagrangian codes. The narrower 250-μm gap (solid line) has a spatial profile similar to the measurement but with a much larger calculated peak n_e value of $\sim 1.2\times 10^{21}$ cm^{-3}. For $D_{\text{gap}}=500$ μm (dashed line), LASNEX predicts a lower peaked n_e value of $\sim 6\times 10^{20}$ cm^{-3}, similar to the measured value, and a comparable stagnation width, but there is a significant difference in the spatial profiles between the calculation and measurement. These calculations disagree with the measured profiles, which show the evolution from interpenetration at early time, to the development of a ''soft stagnation'' with large density buildup at or near the symmetry plane, and expose the deficiency of Lagrangian codes for this type of application.

The dynamics of the counterstreaming plasmas can be more accurately described by multispecie fluid codes [8,16,20,21] or fully kinetic models [10,13,17]. Unlike single-fluid codes that enforce stagnation at the symmetry

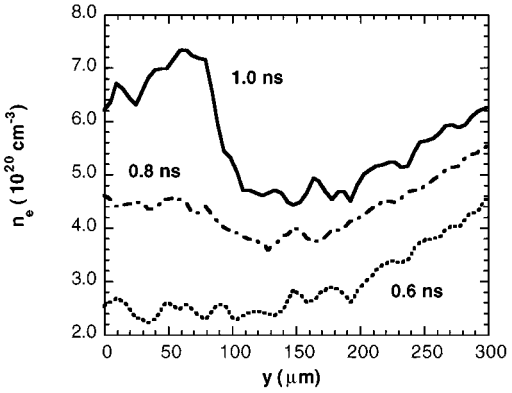

FIG. 5. Calculated 1D n_e lineouts from 2D PIC-calculated profiles 250 μm from the gap for the $D_{\text{gap}}=250$ μm target at three times.

plane, these models follow the interpenetration, slowdown, and eventual stagnation and thermalization of the separate plasma streams. Depending on the collisionality of the plasmas, which in turn depends on temperatures, density, and ionic charge, varying amounts of interpenetration are predicted. The scaling studies of Ref. [16] show that the scaled interpenetration for colliding planar expanding plasmas is weakly dependent on collisionality. In particular, the time for stagnation to occur is nearly proportional to the characteristic expansion time, C_s/D, where C_s is the sound speed and D is the target separation. We expect a similar scaling with the target gap for this 2D geometry.

We have simulated the plasma interpenetration for the experimental geometry using a 2D collisional particle-in-cell (PIC) code; this code is a straightforward generalization of the techniques described in Ref. [16]. Gold plasma (50 times ionized) is injected at the sound speed from the boundaries corresponding to the slab locations with constant flux equal to $n_0 C_s$, where n_0 is the boundary density. These simulations were isothermal ($T_e=3$ keV) with injection parameters motivated by LASNEX simulations. Much like the 1D simulations, we observe initial interpenetration followed by slowing and heating of the separate streams, resulting finally in a ''soft stagnation'' along the midplane. Figure 5 shows n_e lineouts, similar to the lineout taken in Fig. 4(b), with a 250-μm gap at three different times. The initial interpenetration and soft stagnation are evident, and are qualitatively consistent with the experimental data presented in Fig. 4(a). Results from simulations with a 500-μm gap behave as expected from scaling arguments of Ref. [16], namely, that the time for stagnation takes approximately a factor of 2 longer compared to the case with a 250-μm gap.

In summary we have conducted a set of experiments and performed comparable simulations to study the evolution of the collision of high-density, high-temperature plasmas that are of interest to the design of hohlraum targets for ICF applications. We obtained 2D n_e profiles of large-scale-length colliding plasmas using a soft-x-ray laser interferometer. By probing the plasma at different times and by varying target geometries, we obtained a qualitative view of the evolution of the colliding plasma. Our measured n_e profiles show the evolution of the counterstreaming plasmas from interpenetration at early time with no density maximum, to a stagnation where we observe significant n_e buildup at the symmetry plane where the plasmas collide. Varying the gap separations between target slabs results in significantly different spatial features of the measured n_e profiles. We observed a single n_e peak at the symmetry plane with a large gap, and an n_e profile that peaks off the symmetry plane with a narrower gap, which is suggestive of shocks propagating away from the symmetry plane. Scaling the target separation with the time of stagnation, the narrower gap target represents a later time evolution of the colliding plasmas. Single-fluid Lagrangian radiation hydrodynamics codes, such as LASNEX, do not allow for plasma interpenetration and predict an unphysically large T_i with strong shocks propagating away from the symmetry plane. The LASNEX-calculated n_e profile, in the single-fluid approximation, shows comparable stagnation width but with n_e profiles that are peaking off the symmetry plane as soon as the plasma starts to collide, which is characteristic of strongly shock-heated, outward propagating plasmas. Incorporating plasma interpenetration in our predictive codes, such as through multispecie fluids or a PIC kinetic treatments can significantly improve the predictive capability of laser-produced plasmas in a colliding configuration.

Work performed by Lawrence Livermore National Laboratory under the auspices of the U.S. DOE under Contract No. W-7405-ENG-48.

[1] S. W. Haan *et al.*, Phys. Plasmas **2**, 2480 (1995).
[2] J. D. Lindl, Phys. Plasmas **2**, 3933 (1995).
[3] G. B. Zimmerman and W. L. Kruer, Comments Plasma Phys. Controlled Fusion **2**, 51 (1975).
[4] L. V. Powers *et al.*, Phys. Rev. Lett. **74**, 2957 (1995).
[5] W. J. Krauser *et al.*, Phys. Plasmas **3**, 2084 (1996).
[6] R. S. Bosch *et al.*, Phys. Fluids B **4**, 979 (1992).
[7] S. M. Pollaine *et al.*, Phys. Fluids B **4**, 989 (1992).
[8] R. L. Berger *et al.*, Phys. Fluids B **3**, 1 (1991).
[9] C. A. Back *et al.*, Rev. Sci. Instrum. **66**, 764 (1995).
[10] O. Larroche, Phys. Fluids B **5**, 2816 (1993).
[11] M. D. Wilke *et al.*, SPIE Proc. Int. Soc. Opt. Eng. **2523**, 229 (1995).
[12] R. C. Elton *et al.*, Phys. Rev. E **49**, 1512 (1994).
[13] O. Rancu *et al.*, Phys. Rev. Lett. **75**, 3854 (1995).
[14] L. B. Da Silva *et al.*, Phys. Rev. Lett. **74**, 3991 (1995).
[15] A. S. Wan *et al.*, J. Opt. Soc. Am. B **13**, 447 (1996).
[16] P. W. Rambo and J. Denavit, Phys. Plasmas **1**, 4050 (1994).
[17] P. W. Rambo and R. J. Procassini, Phys. Plasmas **2**, 3130 (1995).
[18] M. E. Jones *et al.*, Phys. Plasmas **3**, 1096 (1996).
[19] S. H. Glenzer *et al.*, Phys. Rev. Lett. **77**, 1496 (1996).
[20] C. Chenais-Popovics *et al.*, J. Quant. Spectrosc. Radiat. Transfer **54**, 105 (1995).
[21] M. E. Jones *et al.*, J. Comput. Phys. **123**, 169 (1996).